

# Lawrence Berkeley National Laboratory

## LBL Publications

**Title**

Stochastic nature of magnetic processes studied by full-field soft X-ray microscopy

**Permalink**

<https://escholarship.org/uc/item/0s1904pz>

**Journal**

Current Applied Physics, 18(11)

**ISSN**

1567-1739

**Author**

Im, Mi-Young

**Publication Date**

2018-11-01

**DOI**

10.1016/j.cap.2018.05.004

Peer reviewed

# Stochastic Nature of Magnetic Processes Studied by Full-Field Soft X-ray Microscopy

Mi-Young Im<sup>1,2,3</sup>

<sup>1</sup>*Center for X-ray Optics, Lawrence Berkeley National Laboratory, Berkeley CA94720, USA*

<sup>2</sup>*Department of Emerging Materials Science, Daegu Gyeongbuk Institute of Science and Technology, Daegu 42988, Korea*

<sup>3</sup>*School of Materials Science and Engineering, Ulsan National Institute of Science and Technology (UNIST), Ulsan 44919, Korea*

## Abstract:

In nanomagnetism, one of the crucial scientific questions is whether magnetic behaviors are deterministic or stochastic on a nanoscale. Apart from the exciting physical issue, this question is also of paramount highest relevance for using magnetic materials in a wealth of technological applications such as magnetic storage and sensor devices. In the past, the research on the stochasticity of a magnetic process has been mainly done by macroscopic measurements, which only offer ensemble-averaged information. To give more accurate answer for the question and to fully understand related underlying physics, the direct observation of statistical behaviors in magnetic structures and magnetic phenomena utilizing advanced characterization techniques is highly required. One of the ideal tools for such study is a full-field soft X-ray microscope since it enables imaging of magnetic structures on the large field of view within a few seconds. Here we review the stochastic behaviors of various magnetic processes including magnetization reversal process in thin films, magnetic domain wall motions in nanowires, and magnetic vortex formations in nanodisks studied by full-field soft X-ray microscopy. The origin triggering the stochastic nature witnessed in each magnetic process and the way to control the intrinsic nature are also discussed.

## 1. Introduction

With the high potential of magnetic nanomaterials for applications in advanced nanotechnologies such as high-density recording media, data storage devices, and magnetic sensors [1-7], one of the fundamental and crucial issues is whether a magnetic process is deterministically behaved. This issue is directly linked to the question for the reproducibility of the magnetic process, which is a basic factor for achieving a high and accurate performance in magnetic nanodevices. In years ago, due to limitation in conventional magnetic microscopy techniques providing high spatial resolutions, the stochasticity and/or reproducibility of magnetic processes have been mostly studied by indirect probes such as macroscopic hysteresis loops [8-10]. Therefore, accurate analysis for stochastic and deterministic natures of magnetic processes happened on a nanoscale and comprehensive understanding the related physical principles have not been successfully addressed.

Since characterization techniques offering high spatial resolutions such as X-ray microscopes have been advanced, the stochastic issue has been tackled based on the direct observation of statistical behaviors of magnetic structures and magnetic phenomena on a nanoscale. A representative advanced imaging technique utilizing X-ray sources, which has been actively employed in such research, is a magnetic transmission soft X-ray microscope (MTXM) at Advanced Light Source (XM-1, ALS) [11,12]. This microscope enables direct imaging in-plane and out-of-plane magnetic components with a lateral resolution down to 20 nm provided by state-of-the-art X-ray optics called Fresnel zone plates [12]. In addition, XM-1 is in a full-field mode and thus allows observing magnetic structures on a large of field of view ( $\sim 10 \mu\text{m}$ ) within a few seconds, which is strongly beneficial for the investigation of statistical behavior of magnetic processes and therefore their stochastic natures.

In this article, previous works on stochastic natures of various magnetic processes such as domain nucleation and reversal process in ultrathin CoCrPt alloy films [13,14], the domain-wall motions in  $\text{Ni}_{80}\text{Fe}_{20}$  notched nanowires [15,16], and the creation of vortex structure in  $\text{Ni}_{80}\text{Fe}_{20}$  nanodisks [17-19] studied by soft X-ray microscopy are reviewed. A primary factor affecting the stochasticity in each magnetic process and the approach how to control the intrinsic character, stochastic nature are further discussed.

## 2. Magnetization reversal process in thin films

Nanogranular thin films with perpendicular magnetic anisotropy have been considered as promising candidates for high-density magnetic recording media [20-22]. Repeatable local domain nucleation and reliable magnetic reversal process are key aspects for developing magnetic-based recording technologies [23-26].

In perpendicularly magnetized CoCrPt alloy films, the repeatability of domain nucleation and magnetic reversal process was investigated. Magnetic images in CoCrPt were recorded at the Co  $L_3$  (778 eV) X-ray absorption edge. Fig. 1 (a) shows magnetic domain configurations observed on the identical sample area of  $(\text{Co}_{0.83}\text{Cr}_{0.17})_{87}\text{Pt}_{13}$  alloy film during two consecutive hysteretic cycles. The sample was fully saturated by +3 kOe and then the reverse fields of +512, +383, +254, +124, +5 Oe. One clearly sees that the domain nucleation sites observed in two successive cycles are not identical. The nucleation process of domains is rather stochastic than deterministic in  $(\text{Co}_{0.83}\text{Cr}_{0.17})_{87}\text{Pt}_{13}$  film even with its nanogranular microstructure containing numerous grain boundaries acting as pinning sites. This is more clearly visualized in Fig. 2 (b) where two MTXM images for domain configurations taken at +400 Oe within two consecutive measurements are overlapped.

The same type of experiment was conducted for Barkhausen avalanches [27, 28], which are discrete and sudden jumps occurred during the field-driven magnetization reversal. Figure 2 illustrates representative magnetic configurations recorded at the applied magnetic fields of +400, +200, 0, -200 Oe in two consecutive cycles in  $(\text{Co}_{0.83}\text{Cr}_{0.17})_{87}\text{Pt}_{13}$  (a) and the distributions of Barkhausen avalanches in each field step, I, II, or III where the color codes of green, yellow, and red correspond to the field steps I, II, and III, respectively (b). To visualize the Barkhausen avalanches in each field step, the domain configuration image taken at the initial field of the step was subtracted from that at the final field of the step. It is clearly visible in Fig. 2 (b) that discrete Barkhausen avalanches randomly distributed over the film. The size and shape of Barkhausen avalanches are quite different in the three field steps. In the field step I, small-size Barkhausen avalanches are witnessed while large and elongated avalanches appear as the field approaches the step III, which implies that the mechanism in the Barkhausen avalanches changes accordingly with the variation of the magnetization reversal process from domain nucleation in the step I to domain wall propagation in the step III. More importantly, the distributions of Barkhausen

avalanche considerably transforms in repeated hysteresis cycles as observed in the domain nucleation and magnetization reversal processes [14].

As a reason for the stochastic nature observed in the nucleation and reversal processes of domains in CoCrPt films, thermal fluctuation effect was considered. The random behavior of Barkhausen avalanches in the films was also interpreted to be attributed to a thermal effect which dominates the magnetization reversal process rather than, e.g., defect or grain boundary induced processes. To confirm the effect of thermal fluctuation, nanomagnetic simulations for the magnetization reversal process of CoCrPt alloy films utilizing the stochastic Landau–Lifshitz–Gilbert equation was performed at  $T= 0$  and 300 K [29]. In this equation, the thermal effect is reflected by considering a fluctuating magnetic field, which is caused by fluctuations of the magnetic moment orientation due to interaction of the magnetic moment with conducting electrons, phonons, nuclear spins, etc. The variance of thermal fluctuation is defined by  $V_{ar}=2\alpha k_B T/(1+\alpha^2)\gamma\mu_0 M_s V$ , which is derived from Brown’s Fokker-Planck equation [30]. Here, the  $\gamma$  and  $\alpha$  are a gyromagnetic ratio and a damping parameter and the  $V$  is the island volume. In the simulations, the granular microstructure of CoCrPt sample, i.e., grains segregated by grain boundaries with the size of about 20 nm was reflected.

Magnetic domain configurations at +700, +500, +350, +200, and 0 Oe taken from four consecutive simulations performed at  $T= 300$  K with identical simulation conditions are illustrated in Fig. 3. Note that domain configurations obtained from repeated simulations are not fully correlated as observed in experimental results in Fig.1, which is clearly distinguished from the simulation results obtained at 0 K showing perfect deterministic domain nucleation and reversal process within repeated simulations. The simulation results were also quantitatively compared with the experimental ones by estimation of the correlation coefficient among domain configurations taken from consecutive simulation cycles. The correlation coefficient was found to be in the range from 0 to 0.40 with varying the magnetic field from +700 Oe to 0 Oe, which is in a good agreement with the experimental values from 0.08 to 0.38 with changing the field from +620 to +5 Oe. This result supports that thermal effect is considerably responsible for the stochastic nature of the domain nucleation and reversal process in CoCrPt films.

### 3. Domain-wall motions in nanowires

Magnetic domain wall is a boundary separating magnetic domains. Since the concepts of logic and memory devices utilizing magnetic domain-wall (DW) moving along a nanowire have been introduced [31-34], lots of efforts have been dedicated to studying on current (field)-driven magnetic DW motions. To achieve DW-based logic and memory devices, one of the biggest issues is complete understanding the stochastic character of DW motions. In other words, precise control of DWs is a prerequisite [35-39].

In  $\text{Ni}_{80}\text{Fe}_{20}$  nanowires with notch-shaped artificial pinning sites, the stochastic behavior of DW pinning and depinning was systematically investigated through the direct observation of field-driven DW motions. The geometries of  $\text{Ni}_{80}\text{Fe}_{20}$  nanowires such as the width of wire ( $w$ ), the notch depth ( $N_d$ ), and the thickness of wire ( $t$ ) were varied. Fig. 4 (a) shows the series of magnetic images for DW motions observed in 50 nm thick wires with  $w=100, 200, 400$  nm. The wires were fully saturated by +1 kOe and then the magnetic images were recorded with sweeping the external magnetic fields. The magnetic imaging was performed at Fe  $L_3$  edge (706 eV). The DWs are nucleated in the elliptical pad due to its lower shape anisotropy and they propagate toward notches. DWs are likely pinned at notches because of the pinning force exerted by notches and they are depinned when external force by applied magnetic field overcomes the pinning force. It was confirmed that the pinning probability of DWs are changed with varying the wire width. The probability is found to be decreased from about 92% to 75% of the total number of repeated measurements as the wire narrows from 450 to 250 nm. The stochasticity, i.e. the degree of stochastic nature of DW depinning was also quantitatively investigated by determining the standard deviation  $\sigma$  of the DW depinning field. The standard deviation was obtained by statistical analysis of depinning fields measured from 40 repeated measurements for each wire.

Fig. 4 (b) and (c) demonstrate standard deviations with respect to the wire width and the notch depth, respectively. It is very obvious that the degree of stochastic nature of DW depinning, which is indicated by the standard deviation, considerably depends on the geometry of nanowire. Smaller standard deviation represents the low stochasticity, i.e. high repeatability of DW depinning at the notch. The standard deviation tends to be decreased as the notch depth reduces and the wire gets thicken. It is minimized to below 7 Oe in the wire with the wire width of 150

nm, the notch depth of 50 % of wire width, and the wire thickness of 50 nm. This result implies that the stochastic behavior in the DW depinning is not only influenced by thermal fluctuation effects. The geometry of wires is also very crucial in the determination of the stochasticity of DW depinning process. To find out the other factor causing the stochastic nature of the DW depinning, which is related to the geometry of nanowires, the detailed DW structures pinned at the notched and the depinning field were investigated as displayed in Fig. 5 (a). Note that the microstructure of the DW pinned at the notch can be varied from transverse wall to vortex wall in repeated measurements as indicated by red box and more interestingly, the depinning fields appear to be different depending on the type of the DW. Fig. 5 (b) exhibits various microstructures of the DW observed within repeated measurements performed with identical experimental conditions, which yield different depinning fields. The results in Fig. 5 supports that the stochastic nature of the DW depinning field is induced by the generation of various DW types in the vicinity of a notch, which happens due to the complicate magnetic process near the notch and the interaction between the DW and the notch. Based on the fact that the stochasticity considerably changes with varying the geometry of wires as shown in Fig. 4 (b) and (c), it can be interpreted that the numbers of different DW types, which can be generated at the notch, are different as the geometry of wires changes. This means that the intrinsic stochastic nature of the DW depinning process can be controllable by optimizing the design of nanowires [15,16].

#### **4. Formation of magnetic vortex structures in nanodisks**

Magnetic vortex is a ground state of magnetic configuration created in a micron-size magnetic element in balancing between dipole-dipole interaction and exchange coupling. Magnetic vortex consists of an in-plane circular domain called as chirality rotating clockwise ( $c = +1$ , CW) or counter-clockwise ( $c = -1$ , CCW) and an out-of-plane magnetic component denoted as polarity pointing either up ( $p = +1$ ) or down ( $p = -1$ ) [40, 41]. Magnetic vortices have sparked enormous interests due to their compelling spin structures for understanding fundamental physics of nanospin behavior and also their potential in a wide range of applications such as logic device,

data storage, transistor, signal transferring, and artificial skyrmion crystals [42-46]. In research of magnetic vortices, one of the most crucial topics is a fundamental understanding of non-deterministic behavior in the formation of vortex structure, which is directly related to the control of vortex structure, since it tremendously affects the performance of magnetic vortex-based nanospin devices. There have been some works studying on the control of magnetic vortex structures, but they have been done by a single measurement, which limits the comprehensive understanding the reliability in the control of vortex structures and the relevant physics of non-deterministic nature in the formation of vortex structures.

Control of vortex structures and its reliability were extensively studied based on significantly enough statistic measurements for the formation of vortex structures in asymmetric permalloy (Py, Ni<sub>80</sub>Fe<sub>20</sub>) disks with one-side flat edge. A prior, it has been assumed that circularity would be reliably controlled in asymmetrically shaped magnetic disks. To confirm it, the creation of circularity was directly observed by soft X-ray microscopy. Fig. 6 (a) depicts the representative series of images for circularity created in a Py disk array composing of disks with a radius of  $R = 500$  nm, a height  $h = 40$  nm, and an asymmetry ratio  $r = 0.3R$ , and spaced by the interdisk distance of  $d = 800$  nm within two repeated measurements. An external magnetic field of  $H = +1$  kOe was applied parallel to the flat edges of disks in  $+x$  direction to magnetically saturate the disks and then released them to zero. As can be seen in the images, CW circularity is mostly created in the field sequence,  $H = +1$  to 0 kOe, which is likely due to the asymmetric shape of disks. However, unlike the prior assumption, the created circularity  $c$  in individual disks is not always identical within repetitions, but shows a stochastic character as indicated by yellow circles. The stochastic character in the formation of circularity was also studied in other arrays with different interdisk distances of  $d = 200$  and 500 nm and systematically examined by performing the repeated measurements of the vortex formation more than 40 times in each array. Vortex structures formed in 25 individual disks were investigated in each array. The generation probabilities of CW and CCW circularities in the arrays obtained from the statistical measurements together with the generation probabilities of dominantly (recessively) created circularity, CCW (CW) for the array with  $d = 200$  nm and CW (CCW) for the array with  $d = 800$  nm, are displayed in Fig. 6 (b). Here, the error bars indicate the standard deviations in the generation probabilities of circularities in 25 disks. It is noticeable that the degree of stochasticity, which is a counterpart of the concept of repeatability for the creation of the



identical circularity and is indicated by the generation probability of dominantly created circularity, has a strong correlation with the interdisk distance of disk arrays. The stochasticity is higher in the array with  $d = 500$  nm than ones in the other two arrays with  $d = 200$  nm and  $d = 800$  nm. This observed phenomenon is very interesting since the dependency of the stochasticity on the interdisk distance cannot be explained by thermal fluctuation effects although thermal effect has been assumed as a main factor triggering the stochastic nature in magnetic processes.

To explore the origin of the experimentally witnessed phenomenon, i.e., the V-shaped dependency of the stochasticity on the interdisk distance, we carried out micromagnetic simulations for the formation of vortex structures repeatedly in Py nanodisks with different interdisk distances of  $d = 201$  nm,  $d = 501$  nm, and  $d = 801$  nm while the simulation conditions were kept the same as approached in the experiments. Fig. 7(a) illustrates images for vortex creation process. It is worth noticing that in the disk array of  $d = 501$  nm showing the high stochasticity, various dynamic processes are observed within the repeated simulations even without external stimulators such as thermal noises and more importantly, finally created circularity is different depending on the pattern of dynamics. This simulation results suggest that the higher stochasticity observed in the array of  $d = 500$  nm is dictated by the chaotic dynamics, which only appears in the array. As a reason why the chaotic dynamics occurs only in the disk array with  $d = 500$  nm, the strength of stray fields, which is variable with changing the interdisk distance, was considered. The distribution of stray field and its strength in each disk array are demonstrated in Fig. 7 (b) and (c). The stray field is very strong ( $\sim 94$  Oe) in the array of  $d = 201$  nm and it is pretty weak ( $\sim 25$  Oe) in the array of  $d = 801$  nm while the strength of stray field is in the intermediate value ( $\sim 39$  Oe) within the array of  $d = 501$  nm. It turned out that the intermediate strength of stray field is responsible for the chaotic dynamics only appeared in the array of  $d = 501$  nm and it is tightly related to the locations of (anti-)vortices during the dynamic processes. As shown in Fig. 7 (c), the vortices place in the middle of the disk, which yields various dynamic patterns.

This work demonstrates that ultrafast dynamics at the initial stage of vortex creation can be a decisive factor for the stochastic nature in the formation of vortex structures in asymmetric nanodisks and the stochasticity in the vortex formation process can be controlled by adjusting the geometrical parameter of disk arrays such as interdisk distance [17-19].

## 5. Conclusions

In this review, works on the stochastic nature of various magnetic processes ranging from magnetic reversal and nucleation processes of domains in thin magnetic films, domain-wall motions in  $\text{Ni}_{80}\text{Fe}_{20}$  notched nanowires to the formation process of magnetic vortex structures in  $\text{Ni}_{80}\text{Fe}_{20}$  nanodisk arrays studied by soft X-ray microscopy were summarized. The origin of stochastic nature for each magnetic process was discussed. It became obvious that thermal fluctuation effects, the variety of domain wall types, and the chaotic dynamics of vortex creation are deeply involved in the non-deterministic behavior, i.e. stochastic nature of each process, respectively. It was also demonstrated that the intrinsic stochastic nature can be controlled by optimizing the design of magnetic nanostructures such as the width of nanowires and the interdisk distance of disk arrays.

## Acknowledgements

Authors acknowledge the financial supports from the Korean National Research Foundation (NRF) under the grant numbers of 2012K1A4A3053565, 2016K1A3A7A09005336, 2016K1A3A7A09005241, 2015M3D1A1070465, and 2016M3D1A1027831. This work was supported by the DGIST R&D Program of the Ministry of Science, ICT and Future Planning(18-BT-02). Works at the ALS were supported by U.S. Department of Energy (DE-AC02-05CH11231).

## References

- [1] M. Mansuripur, in *The Physical Principles of Magneto-Optical Recording*, Cambridge University Press, New York 1995, pp. 543–676.
- [2] A. Hulbert, R. Schaefer, in *Magnetic Domains*, Springer, Berlin 1998.
- [3] J. M. Deutsch, A. Dhar, O. Narayan, *Phys. Rev. Lett.* 92 (2004) 227203.
- [4] A. Moser, K. Takano, D. T. Margulies, M. Albrecht, Y. Sonobe, Y. Ikeda, S. Sun, E. E. Fullerton, *J. Phys. D: Appl. Phys.* 35 (2002) R157-R167.
- [5] M. N. Baibich, J. M. Broto, A. Fert, F. Nguyen Van Dau, F. Petroff, *Phys. Rev. Lett.* 61 (1988) 2472-2475.
- [6] R.S. Popovic, J.A. Flanagan, P.A. Besse, *Sensor and Actuators A* 56 (1996) 39-55.
- [7] [Yaojin Wang](#), [Jiefang Li](#), [D. Viehland](#), *Materials Today* 17 (2014) 269-275.
- [8] K. Ohashi, H. Takagi, S. Tsunashima, T. Fujii, S. Uchiyama, *J. Appl. Phys.* 50 (1979) 1611-1613.
- [9] J. R. Petta, M.-B. Weissman, G. Durin, *Phys. Rev. E* 56 (1997) 2776.
- [10] P. Cizeau, S. Zapperi, G. Durin, H. E. Stanley, *Phys. Rev. Lett.* 79 (1997) 4669-4672.
- [11] W. Chao, B. H. Harteneck, J. A. Liddle, E. H. Anderson, D. T. Attwood, *Nature* 435 (2005) 1210-1213.
- [12] W. Chao et al., *Opt Express* 17 (2009) 17669-17677.
- [13] M.-Y. Im, P. Fischer, D.-H. Kim, K.-D. Lee, S.-H. Lee, S.-C. Shin, *Adv. Mater.* 20 (2008) 1750-1754.
- [14] M.-Y. Im, P. Fischer, D.-H. Kim, S.-C. Shin, *Appl. Phys. Lett.* 95 (2009) 182504.
- [15] M.-Y. Im, P. Fischer, *J. Phys.: Condens. Matter* 24 (2012) 024203.
- [16] M.-Y. Im, L. Bocklage, P. Fischer, G. Meier, *Phys. Rev. Lett.* 102 (2009) 147204.
- [17] M.-Y. Im, P. Fischer, K. Yamada, T. Sato, S. Kasai, Y. Nakatani, T. Ono, *Nature Communications* 3 (2012) 983.
- [18] M.-Y. Im, K.-S. Lee, A. Vogel, Jung-Il Hong, Guido Meier, Peter Fischer, *Nature Communications* 5 (2014) 5620.
- [19] M.-Y. Im, K.-S. Lee, A. Vogel, Jung-Il Hong, G. Meier, P. Fischer, *NPG Asia Materials* 9

(2017) e348.

- [20] J.-J. Delaunay, T. Hayashi, M. Tomita, S. Hirono, S. Umemura, *Appl. Phys. Lett.* 71 (1997) 3427-3429.
- [21] D. H. Ping, M. Ohnuma, K. Hono, M. Watanabe, T. Iwasa, T. Masumoto, *J. Appl. Phys.* 90 (2001) 4708-4716.
- [22] A. Perumal, Y. K. Takahashi, K. Hono, *J. Appl. Phys.* 105 (2009) 07B732.
- [23] W. Sadnawanto, Budi Purnama, *J. Phys.: Conference Series* 539 (2014) 012024.
- [24] Patrick W. Granitzka et al., *Nano Lett.* 17 (2017) 2426–2432.
- [25] Andrea Meo et al., *Sci. Rep.* 7 (2017) 16729.
- [26] E. Martinez et al., *Sci. Rep.* 5 (2015) 10156.
- [27] H. Barkhausen, *Z. Phys.* 20 (1919) 401-403.
- [28] K.-S. Ryu, H. Akinaga, S.-C. Shin, *Nat. Phys.* 3 (2007) 547-550.
- [29] J. L. Garcia-Palacios, F. J. Lazaro, *Phys. Rev. B* 58 (1998) 14937.
- [30] W. F. Brown, *Phys. Rev.* 130 (1963) 1677-1686.
- [31] D. A. Allwood, G. Xing, M. D. Cooke, C. C. Faulkner, D. Atkinson, N. Vernier, R. P. Cowburn, *Science* 296 (2002) 2003-2006.
- [32] S. S. P. Parkin, U.S. Patent No. 6834005 2004.
- [33] R. P. Cowburn, *Nature (London)* 448 (2007) 544-545.
- [34] T. Ono, H. Miyajima, K. Shigeto, K. Mibu, N. Hosoi, T. Shinjo, *Science* 284 (1999) 468-470.
- [35] M. Kläui, C. A. F. Vaz, J. Rothman, J. A. C. Bland, W. Wernsdorfer, G. Faini, E. Cambril, *Phys. Rev. Lett.* 90 (2003) 097202.
- [36] M. Hayashi, L. Thomas, R. Moriya, C. Rettner, S. S. P. Parkin, *Science* 320 (2008) 209-211.
- [37] J. Akerman, M. Muñoz, M. Maicas, J. L. Prieto, *Phys. Rev. B* 82 (2010) 064426.
- [38] J. Briones, F. Montaigne, M. Hehn, D. Lacour, *Phys. Rev. B* 83 (2011) 060401 (R).
- [39] K. A. Omari, T. J. Hayward, *Sci. rep.* 5 (2017) 17862.
- [40] T. Shinjo, T. Okuno, R. Hassdorf, K. Shigeto, T. Ono, *Science* 289 (2000) 930–932.
- [41] A. Wachowiak et al. *Science* 298 (2002) 577–579.
- [42] B. Van Waeyenberge et al., *Nature* 444 (2006) 461-464.
- [43] D. Mitin, D. Nissen, P. Schädlich, S.S.P.K. Arekapudi, M. Albrecht, *J. Appl. Phys.* 115 (2014) 063906.

[44] D.S. Han, A. Vogel, H. Jung, K.S. Lee, M. Weigand, H. Stoll, G. Schutz, P. Fischer, G.Meier, S.K. Kim, Sci. Rep. 3 (2013) 2262.

[45] H. Jung, Y.-S. Choi, K.-S. Lee, D.-S. Han, Y.-S. Yu, M.-Y. Im, P. Fischer, S.-K. Kim, ACS Nano 6 (2012) 3712-3717.

[46] L. Sun, R. X. Cao, B. F. Miao, Z. Feng, B. You, D. Wu, W. Zhang, A. Hu, H. F. Ding, Phys. Rev. Lett. 110 (2013) 167201.

## Figure captions

Figure 1. (a) Magnetic domain configurations of  $(\text{Co}_{0.83}\text{Cr}_{0.17})_{87}\text{Pt}_{13}$  alloy film taken at applied magnetic fields of +512, +383, +254, +124, +5 Oe in the descending branch of the major hysteresis loop and (b) the overlapped domain configuration image taken at an applied magnetic field of +400 Oe.

Figure 2. (a) Magnetic domain configurations of  $(\text{Co}_{0.83}\text{Cr}_{0.17})_{87}\text{Pt}_{13}$  alloy film taken at the applied magnetic fields of +400, +200, 0, -200 Oe and (b) distributions of Barkhausen avalanches observed in two successive hysteretic cycles.

Figure 3. The reversal patterns are taken at applied magnetic fields of +700, +500, +350, +200, +100, and 0 Oe in the descending branch of the simulated hysteresis loop for four consecutive hysteretic cycles at  $T = 300$  K.

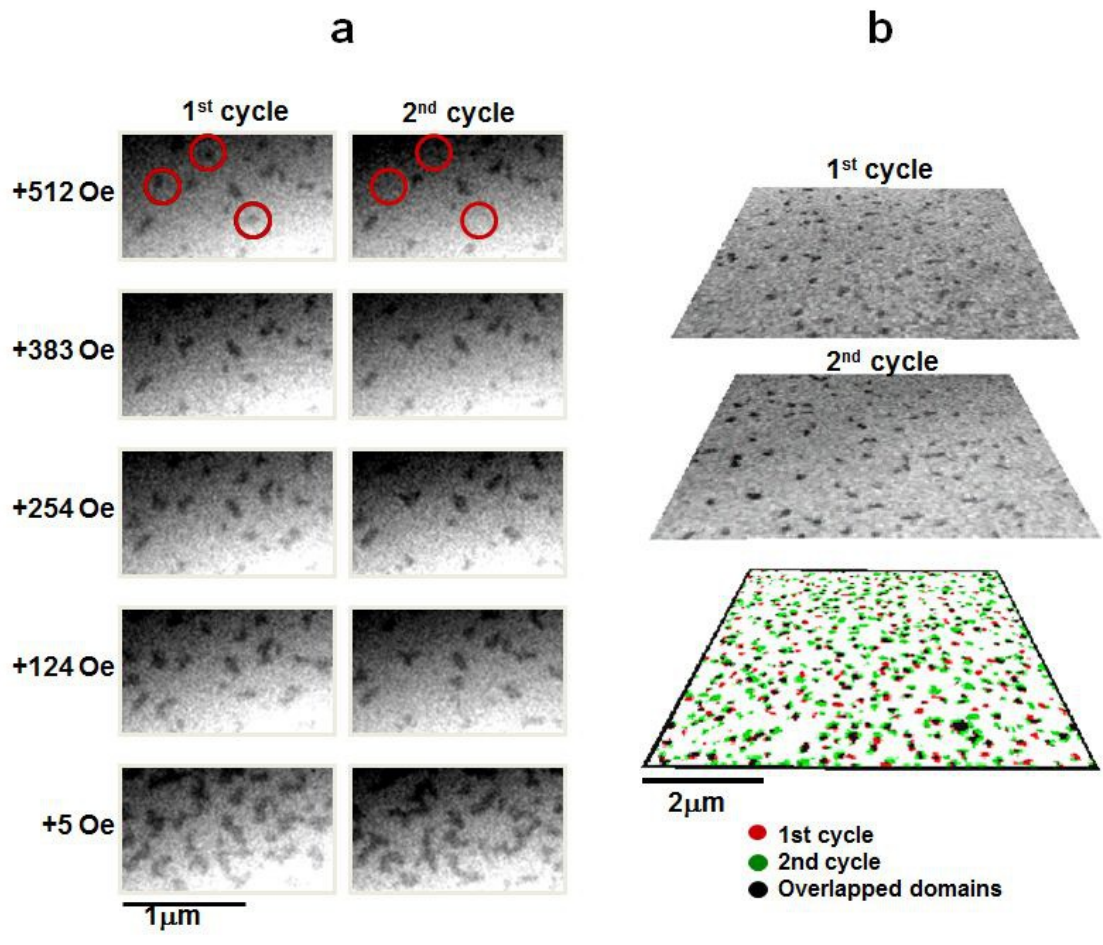
Figure 4. (a) Domain-wall evolution patterns taken from three consecutive experiments under identical measurement conditions for wires of width  $w = 150, 250,$  and  $450$  nm. The color scale represents the field when a domain wall is pinned and depinned at a notch. (b) Standard deviations of the domain-wall depinning field with respect to (b) wire width and (c) notch depth.

Figure 5. (a) Different domain wall structures are observed in the vicinity of a notch just before depinning starts. The notch area is enlarged and shows a transverse DW (top) and a vortex DW (bottom), respectively. (b) Domain walls observed by repeated experiments under identical measurement conditions in a 50 nm thick nanowire of  $w = 250$  nm and  $N_d = 50\%$ .

Figure 6. (a) MTXM images of in-plane magnetic components taken from two successive measurements with the field sweep from +1 kOe to zero in the arrays with the interdisk distance of  $d = 800$  nm. The direction of magnetization is indicated by arrows in the two attached disk

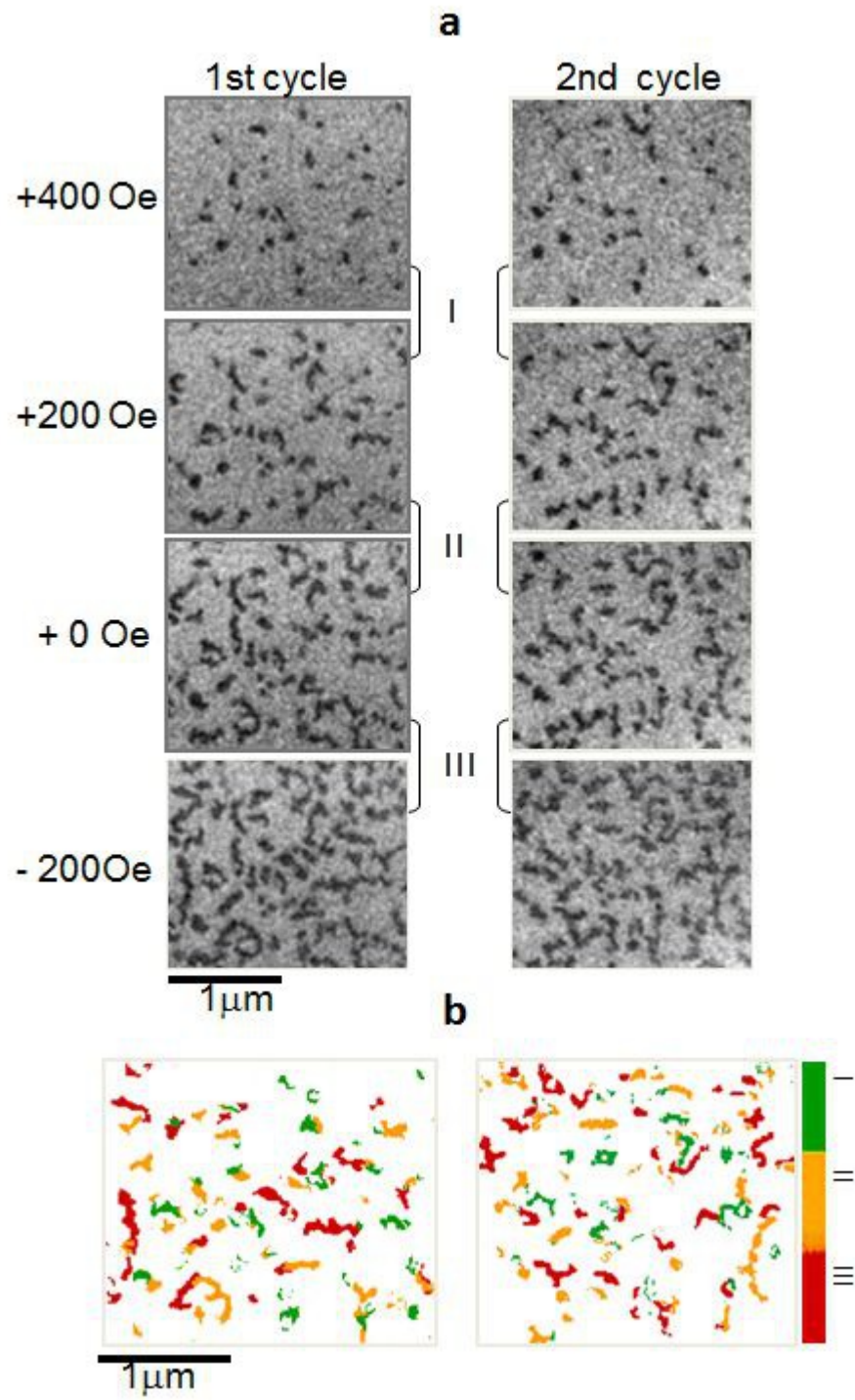
images. (b) The generation probabilities of CW and CCW circularities (majority and minority) as a function of the interdisk distance.

Figure 7. (a) Simulated images for the dynamic process of vortex formation in the disks within the arrays of  $d = 201$  nm,  $d = 501$  nm, and  $d = 801$  nm. (b) The distribution of the stray fields induced by adjacent Py disks with saturated magnetization configuration along  $+x$  direction. The white arrow indicates the direction of the stray fields. The strength of stray fields is represented on the color bar. (c) The magnetization configurations in one half of the disks with  $d = 201$  nm,  $d = 501$  nm, and  $d = 801$  nm at  $t = 17.4$ ,  $14.1$ , and  $12.7$  ns during the dynamic process.



**Fig. 1**





**Fig. 2**

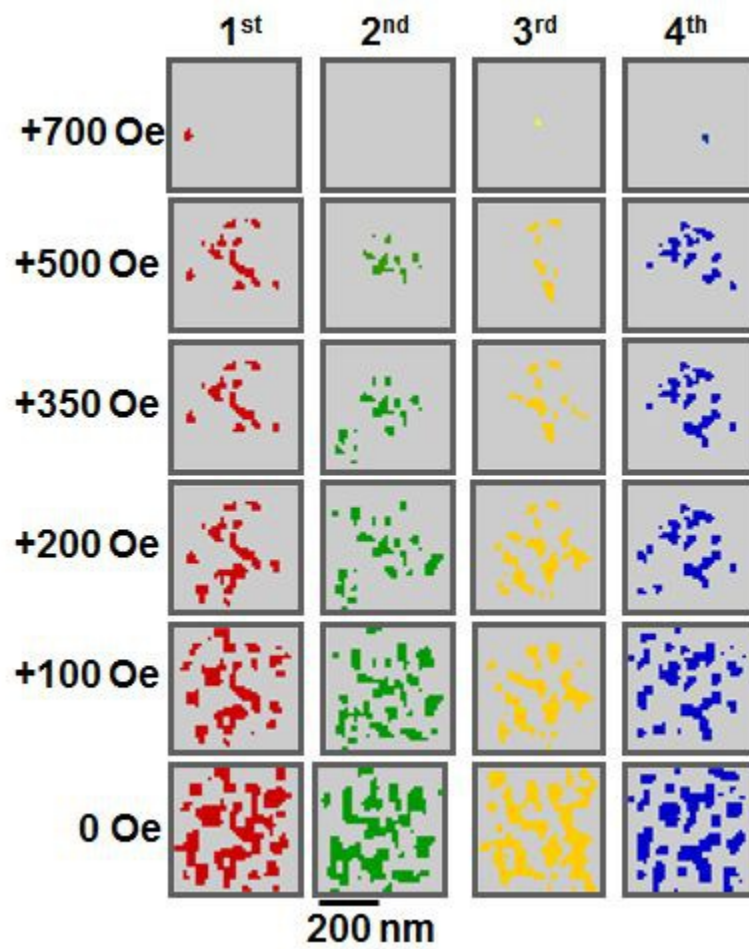
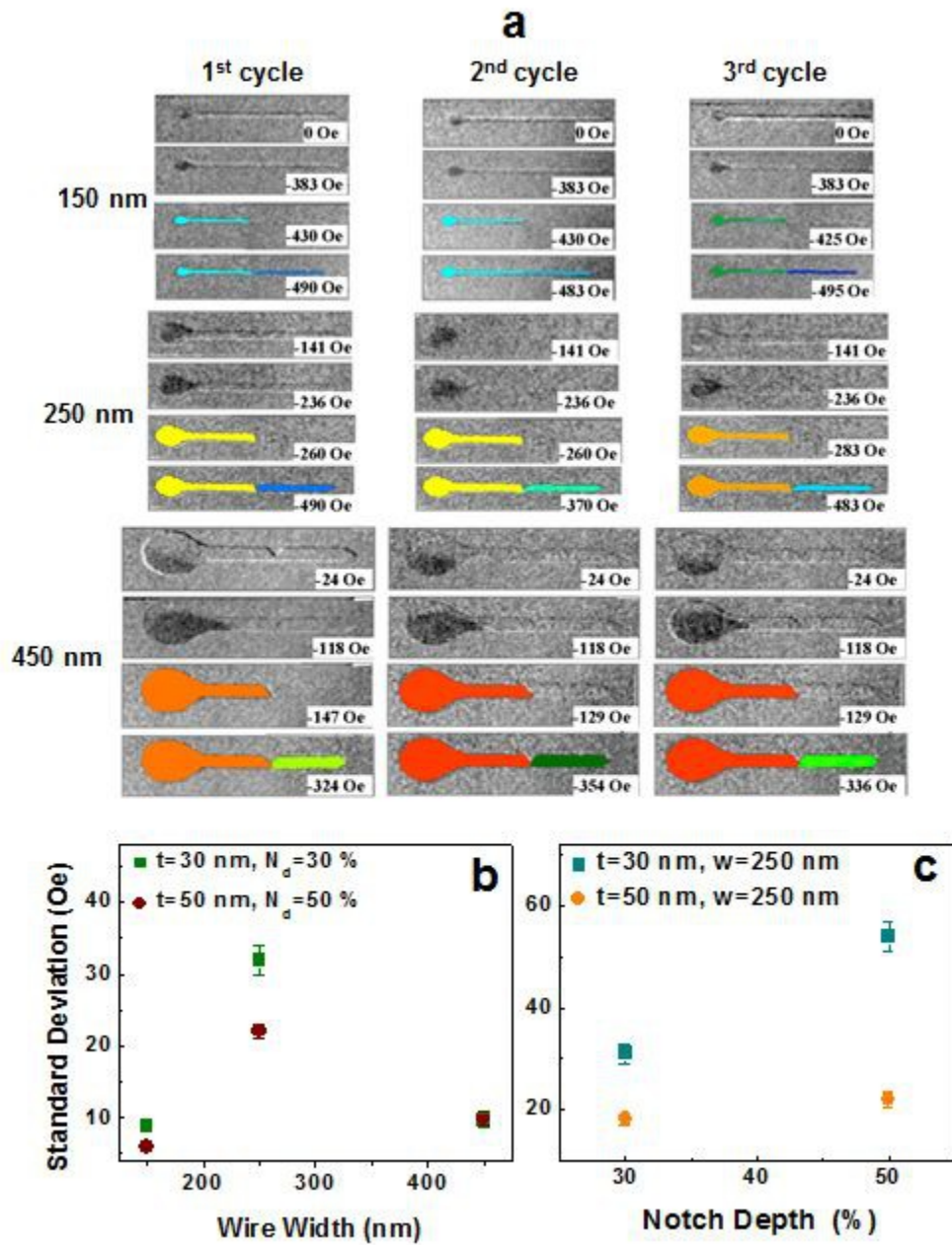
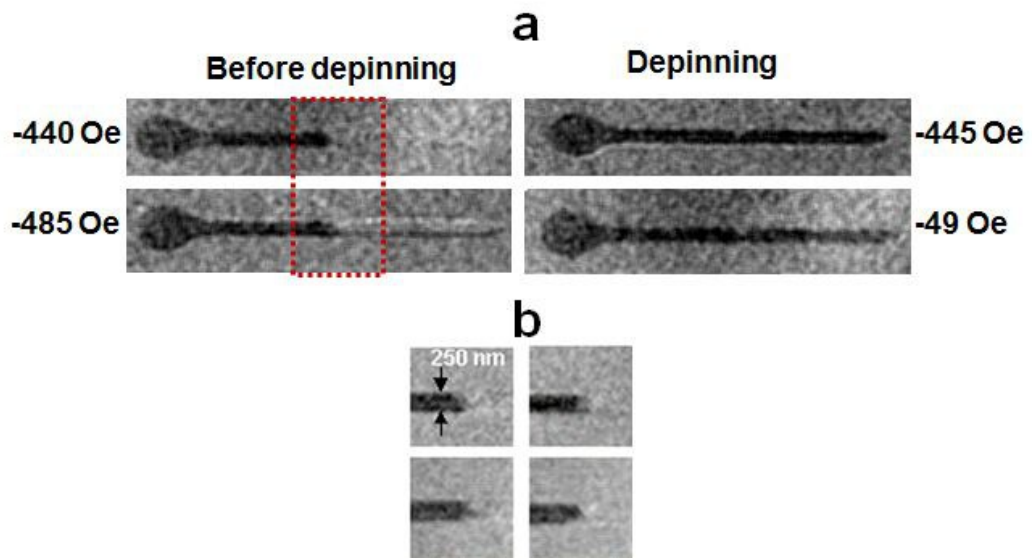


Fig. 3



**Fig. 4**



**Fig. 5**

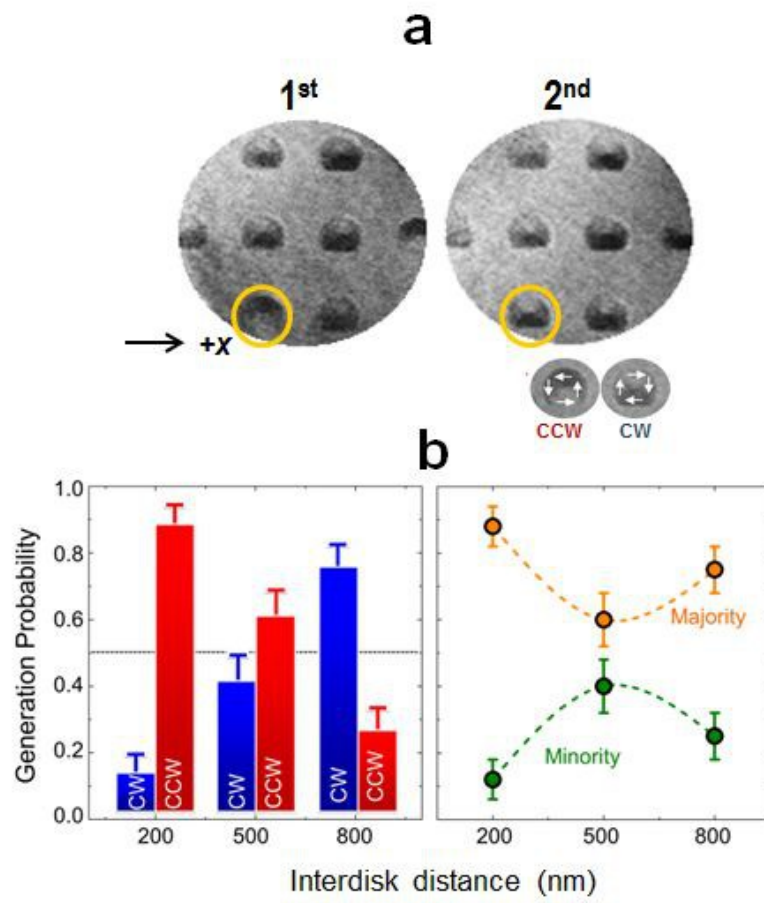


**Fig. 6**

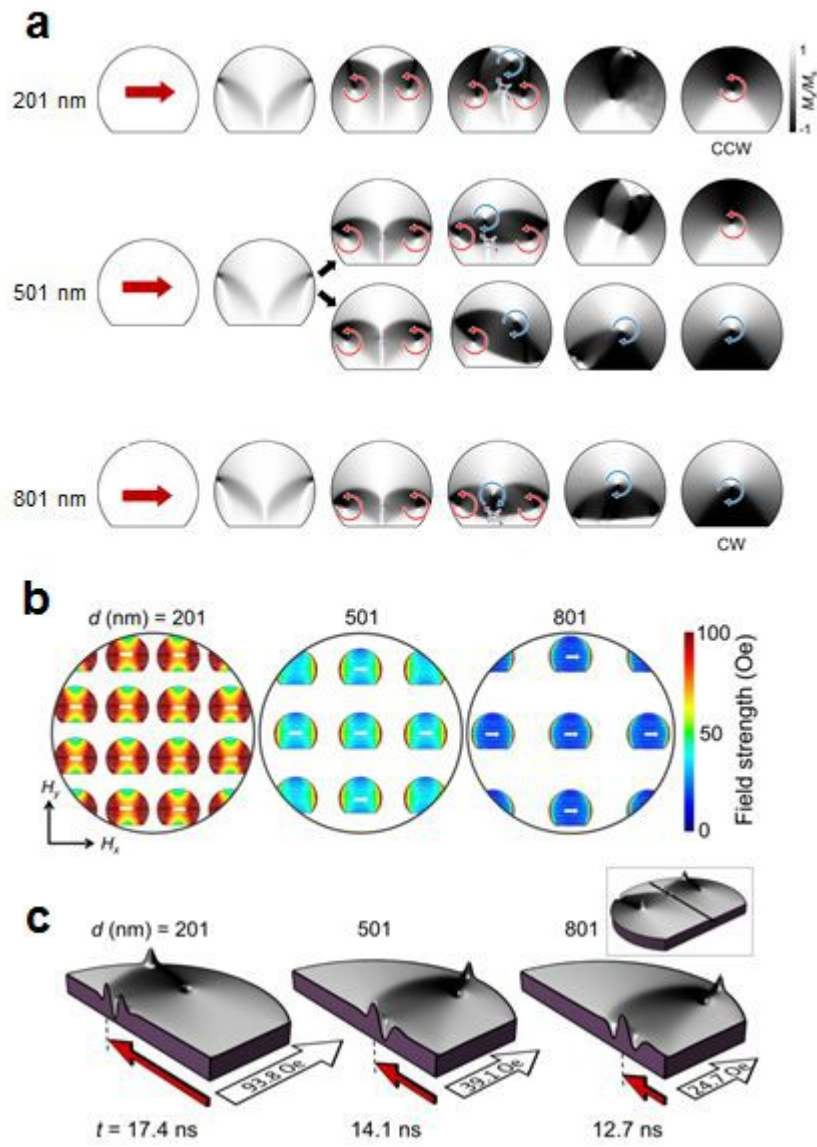


**Fig. 7**